J. Electroanal. Chem., 357 (1993) 201–224
Elsevier Sequoia S.A., Lausanne
JEC 02771

Enhanced electrocatalysis of oxygen reduction on platinum alloys in proton exchange membrane fuel cells *

Sanjeev Mukerjee and Supramaniam Srinivasan

Center for Electrochemical Systems and Hydrogen Research, Texas Engineering Experiment Station, Texas A&M University System, College Station, TX 77843-3402 (USA)

(Received 29 January 1993; in revised form 15 February 1993)

Abstract

Enhanced electrocatalysis of the oxygen reduction reaction (ORR) on carbon-supported binary and ternary alloys of Pt in phosphoric acid fuel cells has been reported previously. This investigation focuses on the electrocatalysis of the ORR on some binary alloys of Pt (Pt+Ni, Pt+Cr and Pt+Co) at interfaces with proton exchange membranes (Dow perfluorinated sulfonic acids). Comparison of the results of these studies with those on carbon-supported Pt electrocatalysts (electrodes containing same Pt loading of 0.3 mg/cm^2) revealed enhanced activities, lower activation energies and different reaction orders for all the alloys. X-ray powder diffraction showed lattice contractions for the alloys, the predominant phase being Pt_3M (LI_2) f.c.c. crystallite. X-ray photoelectron spectroscopy studies on the constituent elements of the electrocatalyst showed no chemical energy shifts owing to alloying and/or the presence of oxides on the surface. Lifetime evaluations of proton exchange membrane fuel cells, using both electrochemical as well as scanning electron microscopy/energy-dispersive X-ray analysis techniques, revealed only small amounts of dissolution of the more oxidizable component during the testing periods, which ranged from 400 to 1200 h. Therefore, the enhanced electrocatalysis exhibited by the binary Pt alloys appears to originate primarily as a result of changes in the lattice structure owing to alloying and the unique environment of the supported catalyst in the particle size range 35–75 Å.

INTRODUCTION

In the 1950s and 1960s, a major contribution was made by Bockris and coworkers [1] on the role of electronic and geometric factors in the electrocatalysis of hydrogen, oxygen and organic electrode reactions, both in respect to the theoretical and experimental aspects. These studies showed that, by using alloy electrocatalysts, the rates of such reactions could be greatly enhanced.

* Dedicated to Professor John O'M. Bockris on the occasion of his 70th birthday and in recognition of his contribution to electrochemistry.

Subsequent studies in the 1970s and 1980s have shown that there are significant improvements in performance in phosphoric acid fuel cells (PAFC) by using alloys of Pt with base transition elements such as V, Cr, Ti instead of Pt as electrocatalysts for the cathodic oxygen reduction reaction (ORR) [2–4]. The alloy electrocatalysts were supported on high surface area carbon, as was the case with Pt electrocatalysts, and were used for the fabrication of porous gas diffusion electrodes. The enhancement of the activity by a factor of 2 to 3 at 180–200°C (the operating temperature range in PAFCs) over that on the carbon-supported platinum electrocatalysts [2,3] has been reported, in spite of the fact that the necessary heat-treatment caused a lowering of the specific Brunauer–Emmett–Teller (BET) surface area from 130 to 50 m^2/g. Thus, in the state-of-the-art PAFCs, binary or ternary alloys of Pt with transition metals serve as electrocatalysts for the ORR.

Even though reports of activity enhancement using supported Pt alloy electrocatalysts in PAFCs date back to the early 1980s, the exact mechanism of their role in the electrocatalysis of oxygen reduction is not yet fully understood. One of the first attempts to elucidate the mechanism involved correlating the electrocatalytic activity with the bond strength of the adsorbate [5]. The Pt–Pt interatomic distance in the alloy was related to the strength of the $M-HO_{2(ads)}$ bond, i.e. the intermediate formed in the rate-determining step of molecular dioxygen reduction

$$O_2 + H^+ + e^- \longrightarrow HO_{2(ads)}$$

This correlation, which can be regarded as a fine tuning of the basic volcano plot [6], was used to show that the lattice contractions resulting from alloying resulted in a more favorable Pt–Pt spacing (while maintaining the favorable Pt electronic properties) for the dissociative adsorption of O_2. Glass et al. [7], in their investigations on the bulk alloys of Pt + Cr (binary alloy at the top of the volcano plot) with different atom percentages of Pt and Cr, showed no such activity enhancement of the ORR. This study indicated a difference in the surface properties of bulk alloys, as compared with the small particles (25–50 Å) in the supported electrocatalysts. Pafett et al. [8] attributed the higher ORR activity on the alloys in phosphoric acid to the dissolution of the more oxidizable alloying component Cr, which led to surface roughening and, hence, an increased surface area. In contrast to these findings on bulk alloys, the supported-alloy electrocatalysts have been reported to retain their non-noble alloying element in the electrode during long periods (6000–9000 h) of operation of PAFCs, despite their instability on thermodynamic grounds [9,10]. Hence, the key of the electrocatalytic behavior of supported alloys must lie in the unique surface properties of the small alloy crystallites on the carbon support.

The effect of some binary alloys of Pt (Pt + Ni, Pt + Co and Pt + Cr) on the electrode kinetics of oxygen reduction in proton exchange membrane fuel cells (PEMFCs) is investigated in this paper. The acid environment in the PEMFCs is different from that of the PAFCs—the anions of the perfluorinated sulfonic acid polymer are only weakly adsorbed on Pt, in contrast to the phosphate anions, which are strongly adsorbed. Furthermore, the PEMFCs operate at less than

100°C, as compared with the PAFCs, which operate at twice this temperature. A comparative study of the electrode kinetic parameters, activation energies, reaction orders for ORR, electrochemically active surface areas and stabilities, was carried out with the PEMFCs and the carbon-supported Pt and Pt alloy electrocatalysts (all electrodes used in this work contain the same Pt loading of 0.3 mg/cm^2). Finally, a combination of some X-ray techniques, such as powder X-ray diffraction, (XRD), scanning electron microscopy/energy-dispersive X-ray analysis (SEM/EDAX and X-ray photoelectron spectroscopy (XPS) were used to examine (i) the type and lattice parameters of the alloys, (ii) the stability (in terms of any dissolution of the more oxidizable alloying component) and (iii) the nature of the surface species together with changes in their valence state.

EXPERIMENTAL

Electrocatalyst specifications and electrode fabrication

The choice of the three alloys (Pt + Cr, Pt + Ni, Pt + Co) was based on the observation that they lie in the upper region of the volcano plot [6], with Pt + Cr being at the highest point. From a crystallographic point of view, all three alloys form super–lattices with the cubic f.c.c. LI_2 structure [13] and the stoichiometry of Pt_3M (where M is the non-noble metal alloying component). The regular termination of the bulk LI_2 crystal structure, normal to the three major crystal axes, results in a variety of surface compositions, starting from pure Pt (⟨200⟩ and ⟨220⟩ planes), 25% M (⟨111⟩ plane) and 50% M (⟨100⟩ and ⟨110⟩ planes). Hence, in these superlattices, it is possible to have surfaces with a higher concentration of M than that in the bulk, i.e. surface enrichment without surface segregation. Such enrichment has been reported previously in respect to the equilibrium surface composition of three Pt_3M systems with Ti [14], Co [15] and Sn [16].

Fuel cell electrodes containing the three carbon-supported binary alloy electrocatalysts were custom-made by ETEK Inc. (Framingham, MA, USA) and these were used in our experiments. The three electrocatalysts were alloyed at 900°C under an inert atmosphere. The electrocatalyst loading was 20% on the high surface area carbon (Vulcan XC-72) and the electrodes contained 0.3 mg/cm^2 Pt (as confirmed by atomic absorption spectroscopy). Electrodes with carbon-supported Pt electrocatalysts (same Pt loading of 0.3 mg/cm^2) were also prepared for control experiments. The choice of an electrocatalyst loading on carbon of 20% was based on the results of previous investigations [11,12], which had shown that this composition is optimum in terms of performance dependence on particle size and reaction layer thickness.

Preparation of membrane and electrode assembly

As described in previous papers [17], the electrodes were impregnated with Nafion® solution (Nafion® 1100, 5% by weight, in a mixture of lower alcohols, Aldrich Chemicals) using a brushing technique. This was followed by air-drying at

80°C and weighing of the electrodes to ensure a Nafion loading of approximately 0.6 mg/cm^2. A Dow membrane (XUS 13204.10, developmental fuel cell membrane) was pretreated by heating first in high purity water (Continental water purification system, Modulab type 1) and secondly in a 5 vol.% aqueous solution of H_2O_2 (J.T. Baker) for 1 h at about 70–80°C to remove organic impurities. The membrane was then treated with 0.5 M H_2SO_4 (J.T. Baker) at 70–80°C for the same time duration. Finally, the H_2SO_4 was removed by repeated treatment in boiling water. The electrodes were then hot pressed to the membrane at a pressure of 70 atm and temperature of 155°C for 90 s. This temperature was chosen because it is close to the glass transition temperature of the Dow membrane.

Assembly of the single cell and its installation in the test station

The membrane and electrode assembly (MEA) was then incorporated into the single-cell text fixture. The details of the MEA and single-cell test fixture have been described elsewhere [18]. A platinized-platinum electrode, located in the anode compartment, served as the reference hydrogen electrode (RHE). The single cell was then installed in the fuel cell test station. The test station was equipped for temperature control of the cell and reactant gases, humidification of the reactant gases and control of the gas flow rates (using a rotameter, Matheson). The total pressure of the gas was regulated using back-pressure regulators (Matheson). Electrical leads from the test station were connected to a programmable power supply (Hewlett Packard model 6033 A) which was interfaced with an IBM/PS2 personal computer for data acquisition, plotting and analysis.

Electrode kinetic and cyclic voltammetric experiments

Prior to the electrochemical performance evaluation, it is essential to attain the optimum operating conditions (with respect to the conditioning of the electrodes, water content of the membrane, humidification conditions and removal of organic impurities), because, when a single cell is assembled, the proton exchange membrane is in a dry state. For this purpose, the cell was maintained at 50°C with the hydrogen and oxygen gases (1 atm) humidified at 60°C and 55°C, respectively, while it was operated at a current density of 200 mA/cm^2 for the first 24h. After this period, the cell temperature was raised to 85°C, the reactant gas pressure to 5 atm and the temperature in the H_2 and O_2 humidification bottles to 95°C and 90°C respectively. It was then operated for 8 h at a current density of 2 A/cm^2, for equilibration with the product water, to attain optimal water absorption conditions with the proton exchange membrane. After this, the measurement of the cell and half-cell potentials vs. the current densities were made using the programmable power supply interfaced with the computer. The pressure and temperature ranges investigated were 1–5 atm and 40–80°C respectively. Comparisons of the *IR*-corrected Tafel plots for the ORR were made at 5 atm and 95°C with the oxygen and hydrogen gases being humidified at 100 and 105°C.

After the potential vs. current density measurements, hydrogen was passed through the counter electrode chamber and argon through the working electrode (cathode, oxygen electrode) compartment, and the electrodes were subjected to potential cycling (50 times) at 25 mV/s. Cyclic voltammetry (CV) measurements were then recorded to determine the electrochemically active surface areas. The tested ranges of the potential and sweep rates were 120 mV to 1 V vs. RHE and 10–50 mV/s respectively. Lower sweep rates are preferred for the measurement of the coulombic charge, owing to hydrogen adsorption or desorption, so as to minimize the pseudo-transmission-line effects in the porous electrode. The electrochemically active surface area of the electrode was obtained from the charge required for hydrogen desorption from the Pt electrocatalyst.

Lifetime evaluations were carried out in the single cells at 50°C (cell temperature), while the humidification temperatures for H_2 and O_2 gases were 60 and 55°C. The cell was maintained at a constant current density of 200 mA/cm^2 and the potential was monitored as a function of time, which ranged from 400–1200 h.

Physico chemical characterization

A variety of X-ray techniques was used. The alloy characteristics (formation of superlattices) and lattice parameters were determined using powder XRD. SEM/EDXA techniques were used to detect dissolution of the alloys by conducting the experiments on the sample before and after the electrochemical investigation. The surface species present and changes in the valence states of Pt owing to alloying were examined using XPS.

The XRD analysis of the supported electrocatalysts were performed using a Siefert-Sintag automated diffractometer with a Cu Kα radiation source. The powdered electrocatalyst samples were kept in a quartz block with dimensions 2.5 cm $\times$ 2.5 cm $\times$ 1 mm. The powders were pressed onto the quartz block using a glass slide to obtain a uniform distribution of powder. The diffractometer was interfaced with a PDP 11/23 computer. The 2θ Bragg angles were scanned over the range of 0°–80°. The diffraction patterns were analyzed by comparing them with standard ASTM powder diffraction files. The SEM/EDXA investigation was conducted using a JSM scanning microscope and Tracor Northern Series 2 energy-dispersive spectroscope with a Z-max window for lighter elements. For this purpose, the membrane and electrode assembly was sliced and mounted on a special platform, which enabled the anode membrane–cathode cross-section to be analyzed. The SEM images were first observed at different points along the cross-section. This was followed by EDXA. The EDXA spectrum was recorded at several points along the cross-section by moving the sample under the electron beam using an x–y manipulator.

The XPS investigation was carried out using a Perkin–Elmer 5500 Auger/ESCA system. The spectrum of the sample was recorded using an Mg $K\alpha$ radiation source and a hemispherical electrostatic energy analyzer. The samples were introduced into the chamber using a rapid introduction probe. The pressure in the

vacuum chamber during analysis was lower than 5×10^{-8} Pa. The binding energy scale was checked using the separation between the Cu 2p and 3p photoelectron lines. The absolute binding energy was referenced to the C 1s line at 284.6 eV. For analysis, the electrocatalyst in powder form was pressed at 650 atm into a pellet 1 cm in diameter. The XPS data acquisition, plotting and analysis were carried out using an Apollo Domain series 3000 (model 3010) computer and PHI-ACCESS software.

RESULTS AND DISCUSSION

XRD studies—crystalline structures of alloys

XRD is a powerful technique for determining the crystalline structure and estimating the particle size of the dispersed metal crystallites. The XRD patterns of the Pt + Ni, Pt + Co, and Pt + Cr alloys (Fig. 1) indicate that all three alloys predominantly form superlattices of the LI_2 type (or $AuCu_3$ type). As indicated by the 2θ positions of the ⟨111⟩, ⟨200⟩ and ⟨220⟩ diffraction lines, superlattices of the type Pt_3Ni, Pt_3Cr and Pt_3Co are the primary phases. However, contributions from other phases are also evident: the Pt + Cr alloy has a 20% contribution from the PtCr phase with an $L1_0$ (AuCu) type of structure; the XRD patterns of the Pt + Co and Pt + Ni alloys also indicate contributions to the extent of 25% from the PtCo and PtNi phases with the $L1_0$ structure. The predominant Pt_3M phases present in the alloys have f.c.c. crystal structures. The lattice parameters for these superlattices were obtained using the 2θ positions of the ⟨111⟩, ⟨200⟩ and ⟨220⟩ diffraction lines. The characteristics of the Pt and Pt alloy electrocatalysts, as obtained from the XRD studies, are summarized in Table 1. As can be seen from this table, alloying of Pt with each of the three transition metals causes a contraction in the lattice parameters. These results are in agreement with previously reported data [20–22].

The particle sizes, based on X-ray line broadening, were estimated using the Scherrer equation [23] and line-width at half-maximum intensity, corrected for instrument broadening, using the Warrens equation [24]. The particle size estimates were based on the peak broadening of the ⟨111⟩ diffraction line relative to that for a bulk Pt foil [25]. The alloying causes an increase in the particle size in the order Pt < Pt + Ni < Pt + Cr < Pt + Co (Table 1).

Electrode kinetic parameters for oxygen reduction at an operating temperature of 95°C and pressure of 5 atm

Approaching the end of the linear region of the half-cell (or single-cell) potential E vs. current density j data for low temperature fuel cells (PEMFC, AFC, PAFC) correspond to the equation

$$E = E_0 - b \log j - Rj \tag{1}$$

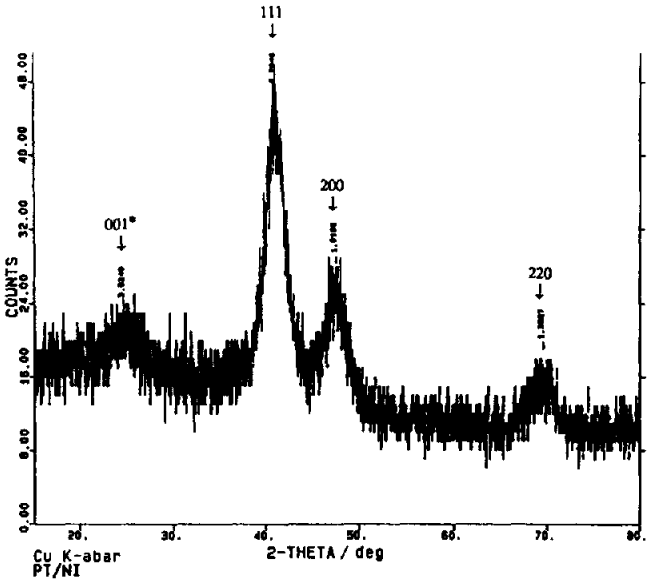

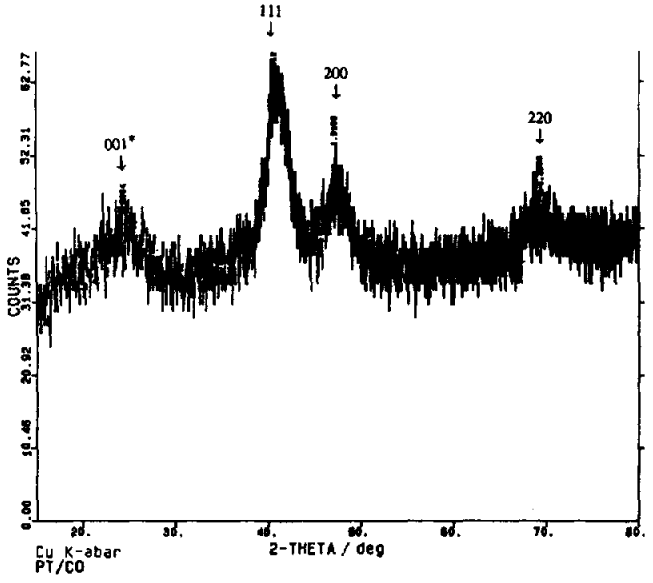

Fig. 1. XRD spectra for (a) a Pt+Ni alloy electrocatalyst with primary phase Pt_3Ni (LI_2) and secondary phase PtNi ($L1_0$) (*), (b) a Pt+Co alloy electrocatalyst, with primary phase Pt_3Co (LI_2) and secondary phase PtCo ($L1_0$) (*), and (c) a Pt+Cr alloy electrocatalyst, with primary phase Pt_3Cr (LI_2) and secondary phase PtCr ($L1_0$) (*).

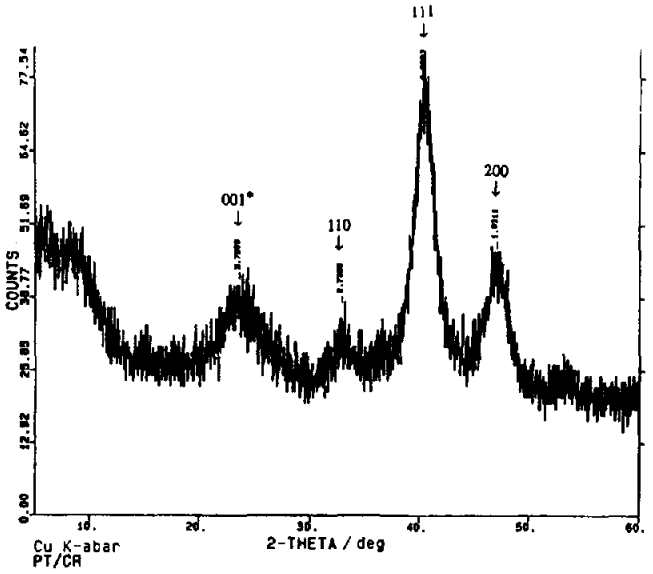

Fig. 1 (continued).

where

$$E_0 = E_r + b \log j_0 \quad (2)$$

In eqns. (1) and (2), j_0 is the exchange current density for oxygen reduction, b is the Tafel slope, E_r is the reversible potential for the oxygen electrode reaction and R represents the resistance (predominantly the ohmic resistance of the electrolyte) responsible for the linear variation of the potential vs. current density plot. At very high current densities, the departure of the E vs. j data from eqn. (1) is due to the onset of mass transport limitations. The parameters E_0, b and R were evaluated

TABLE 1

Characteristics of the Pt and Pt alloy electrocatalysts supported on carbon, with the same Pt loading (0.3 mg cm^{-2}), from XRD studies

Electrocatalyst	Composition/ at.%	Principal phase	Secondary phase	Lattice parameter /Å	Average particle size/Å
Pt+C	–	Pt	–	3.927	35
Pt+Ni	75(Pt)/25(Ni)	Pt_3Ni (LI_2)	PtNi ($L1_0$) 25%	3.812	48
Pt+Cr	75(Pt)/25(Cr)	Pt_3Cr (LI_2)	PtCr ($L1_0$) 20%	3.877	66
Pt+Co	75(Pt)/25(Co)	Pt_3Co (LI_2)	PtCo ($L1_0$) 25%	3.854	75

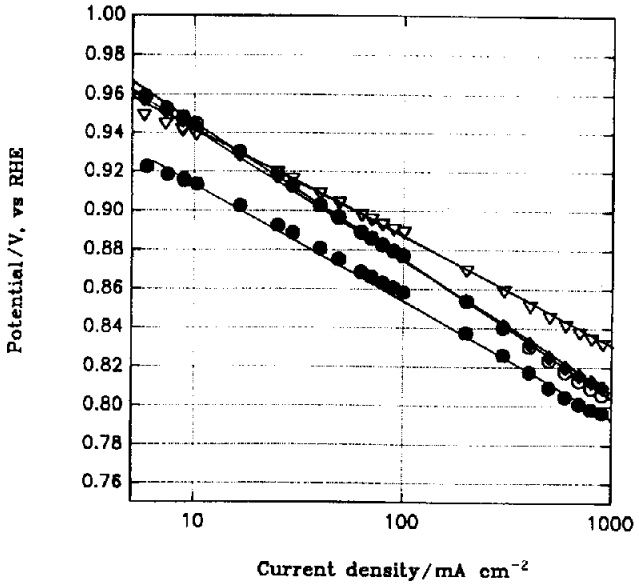

Fig. 2. *IR*-corrected Tafel plots for oxygen reduction in proton exchange membrane fuel cells at 95°C and 5 atm on Pt and Pt alloy electrocatalysts: Pt loading in electrodes, 0.3 mg cm^{-2}; Pt (●); Pt + Ni (○); Pt + Co (◆) and Pt + Cr (▽).

by a non-linear least-squares fitting of eqn. (1) to the experimental data. Using the R values, the jR-corrected Tafel plots [$(E + jR$ vs. log $j)$] were constructed.

A comparison of the jR-corrected Tafel plots for oxygen reduction (as shown in Fig. 2) on the carbon-supported Pt and the binary alloys of Pt with Cr, Co and Ni (20% metal alloy crystallite on carbon, with Pt content in electrodes maintained at 0.3 mg cm^{-2}) shows that there is an enhancement of the electrocatalytic activity of the ORR on all the alloys, based on the geometric areas of the electrodes. The electrode kinetic parameters are presented in Table 2. The current densities at 0.9 V vs. RHE indicate an increment of 23.8 mA/cm^2 for the Pt + Co alloy, 25.5

TABLE 2

Electrode kinetic parameters for oxygen reduction in proton exchange membrane fuel cells at 95°C and 5 atm, using Pt and Pt alloy electrocatalyst. Pt loading in electrodes, 0.3 mg cm^{-2}

Electrocatalyst	E_0/mV	b/mV decade^{-1}	R/Ω cm^{-2}	j_0/mA cm^{-2} ×10^4	j_{900}/mA cm^{-2}	Roughness factor/ cm^2 cm^{-2}	j_{900} [a]/ mA cm^{-2}	j_0 [a]/ mA cm^{-2} 10^5
Pt	982	63	0.14	3.46	22.1	61	0.36	0.57
Pt + Ni alloy	1009	66	0.10	12.5	47.6	56	0.85	2.23
Pt + Cr alloy	997	62	0.10	5.6	52.4	48	1.09	1.16
Pt + Co alloy	1007	65	0.09	10.7	45.9	35	1.31	3.05

[a] Normalized with respect to the electrochemically active surface area.

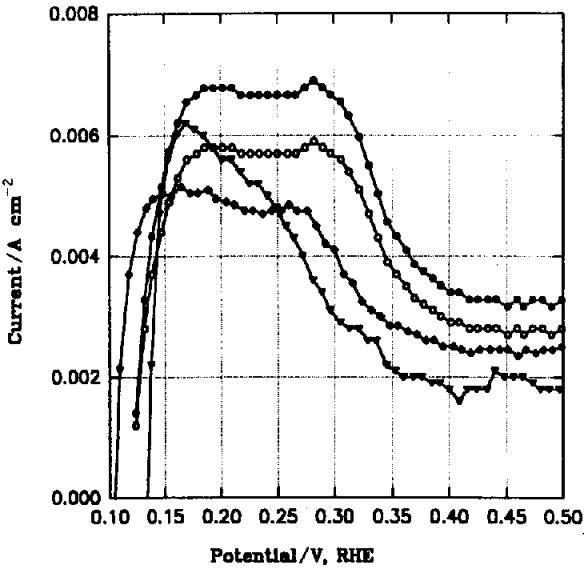

Fig. 3. Hydrogen desorption regions of the cyclic voltammograms at a scan rate of 25 mV s^{-1} for the electrodes in proton exchange membrane fuel cells with the Pt and Pt alloy electrocatalysts (Pt content in electrodes, 0.3 mg cm^{-2}). Roughness factor for Pt (●) 61, Pt + Ni (○) 56, Pt + Co (♦) 35 and Pt + Cr (▽) 48 cm^2 cm^{-2}.

mA/cm^2 for the Pt + Ni alloy and 30.3 mA/cm^2 for the Pt + Cr alloy over that on Pt (Table 2). The potentials at 10 mA/cm^2 show a similar trend and correspond to the increases in current densities at 0.9 V, i.e. an approximately twofold activity enhancement owing to alloying in the case of the three alloy systems. With such activity enhancement on a geometric area basis, it is important to evaluate the activity increments on the basis of the true surface area.

For this purpose, the results of the CV experiments on the three supported alloy electrodes and on the supported Pt + C electrode were used to determine the electrochemically active surface areas. Figure 3 shows the hydrogen desorption regions of the CV results, scanned between a potential range of 120 mV and 1.2 V at a scan rate of 25 mV/s, with the cell operating conditions of 95°C and 5 atm. The coulombic charge for oxidation of the adsorbed atomic hydrogen (area under the anodic peak minus the double layer charge at 0.4 V vs. RHE) was used to evaluate the roughness factor of the electrode, assuming a value of 220 $\mu C/cm^2$ for the oxidation of adsorbed atomic hydrogen on a smooth Pt surface. Table 2 shows the values of the exchange current densities (j_0) and current densities at 900 mV vs. RHE, based on the geometric and real surface areas of the electrodes. On a real surface area basis, Pt + Co and Pt + Cr show better activities at 900 mV vs. RHE than that for the Pt + Ni alloy. Even on a real surface area basis, all the alloys show two- to threefold increases in their activities for the ORR compared with that on the Pt + C electrode (with the same Pt content).

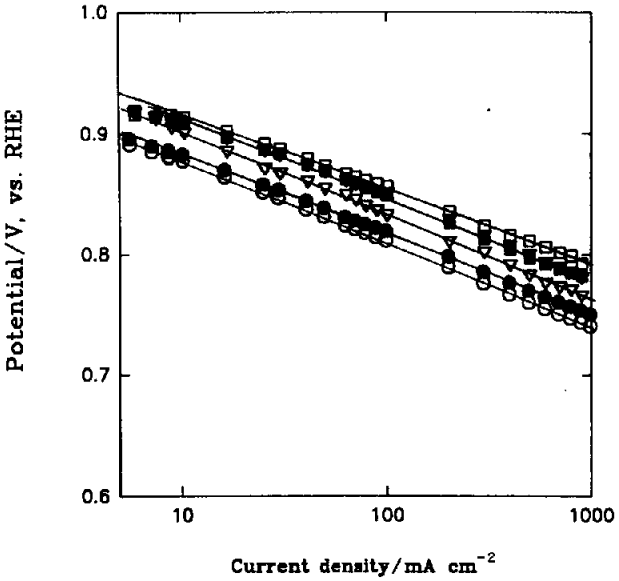

Fig. 4. Dependence of *IR*-corrected Tafel plot on temperature for oxygen reduction at a Pt electrocatalyst in a proton exchange membrane fuel cell: cell pressure, 1.37 atm; temperature, 35 (○), 40 (●), 50 (▽), 60 (▼), 70 (■) and 80°C (□).

Effect of temperature on electrode kinetic parameters

Figures 4 and 5 show representative *IR*-corrected Tafel plots for oxygen reduction on the Pt (0.3 mg/cm^2) and Pt + Ni alloy electrodes as functions of temperature. The effect of the temperature on the electrode kinetic parameters (E_0, b, R and j_{900}) is indicated in Table 3. The increase in temperature from 35 to 80°C causes a minimal variation of the Tafel slopes. The variation is between 2 and 5 mV for the Pt + Ni, Pt + Co, and Pt-containing electrodes and is 6 mV for the Pt + Cr electrode. However, the variation in the value of E_0 over this temperature range is much higher for the Pt electrode ($\Delta E_0 = 43$ mV) than the values for the alloy electrodes (Pt + Cr, $\Delta E_0 = 10$ mV; Pt + Co, $\Delta E_0 = 19$ mV; Pt + Ni, $\Delta E_0 = 12$ mV). A similar trend is found in the values of j_{900}.

Figure 6 shows the plots of log j_0 vs. $1/T$ (the values of j_0 were calculated taking into consideration the necessary corrections for variations in the reversible potential (E_r) for oxygen reduction with temperature). The activation energy ΔE^*, evaluated from these Arrhenius plots is higher for the Pt electrocatalyst ($\Delta E = 75.9$ kJ/mol) than for the alloys Pt + Cr (23.2 kJ/mol), Pt + Ni (27.5 kJ/mol) and Pt + Co (57.0 kJ/mol). The lower activation energies reflect the possibility of a change in reaction mechanism owing to alloying. The analysis, using the values of $R(\delta \log j_{900}/\delta T^{-1})$, also gave very similar results (Table 4).

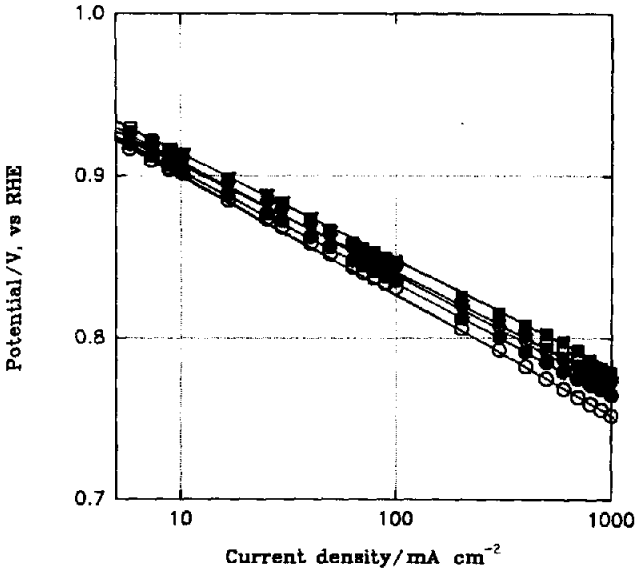

Fig. 5. Dependence of *IR*-corrected Tafel plot on temperature for oxygen reduction at a Pt+Ni alloy electrocatalyst in a proton exchange membrane fuel cell: cell pressure, 1.37 atm; temperature, 35 (○), 40 (●), 50 (▽), 60 (▼), 70 (□) and 80°C (■).

Effect of pressure on electrode kinetic parameters

Figures 7 and 8 represent the *IR*-corrected Tafel plots for oxygen reduction, at several pressures, for the Pt (0.3 mg/cm^2) and Pt + Ni alloy electrodes (with the same Pt loading). Although the effect of temperature on Tafel slopes is negligible, as indicated in the previous section, the effect of pressure on the Tafel slopes is more significant. The values of the electrode kinetic parameters for Pt (0.3 mg cm^{-2}) and for the binary alloys of Pt are given in Table 5 as functions of pressure. The plots of log(exchange current density) (calculated after correction for the variation of the reversible potential with pressure) vs. log(oxygen pressure) (after correction for the vapor pressure of water) are presented in Fig. 9.

The reaction orders, obtained from the slopes of these lines, are unity for both Pt (0.3 mg cm^{-2}) and Pt + Cr alloys; however, for the Pt + Ni and Pt + Co alloy electrodes, lower values of the reaction order (0.79 and 0.77 respectively) were obtained (Table 4). For an nth-order reaction, it can be shown that, at any current density j, we have

$$(\delta E/\delta \log P_0)_j = bnO_2 \tag{3}$$

In this equation b is the Tafel slope, E is the potential at the current density j and P_0 is the oxygen pressure (corrected for the vapor pressure of water). For the ORR on the alloy electrocatalysts, the values of n calculated from the slopes of the E vs. log P_0 plots were not the same as those obtained from the log j_0 vs.

TABLE 3

Effect of temperature on electrode kinetic parameters for oxygen reduction on Pt and Pt alloy electrocatalysts in proton exchange membrane fuel cells. Pt loading in electrode, 0.3 mg cm^{-2}

Electrocatalyst	Temperature/°C	E_0/mV	b/mV decade^{-1}	R/Ω cm^2	j_{900}/ mA cm^{-2}
Pt	40	923	66	0.25	1.2
	50	928	65	0.22	3.4
	60	958	66	0.14	7.6
	70	962	65	0.14	12.8
	80	966	64	0.13	17.7
Pt + Ni	35	972	71	0.20	6.6
	40	975	70	0.19	8.2
	50	978	69	0.16	12.4
	60	981	69	0.14	14.4
	70	981	68	0.13	16.8
	80	984	68	0.13	19.2
Pt + Cr	35	957	70	0.13	2.9
	40	961	69	0.11	5.6
	50	964	68	0.10	8.4
	60	964	67	0.09	12.2
	70	965	66	0.09	16.1
	80	967	64	0.08	19.4
Pt + Co	40	975	62	0.20	8.4
	50	976	63	0.14	12.4
	60	982	63	0.12	15.2
	70	988	64	0.10	19.4
	80	994	64	0.10	24.8

log P_0 plots. It may be more realistic to calculate the reaction orders by using the values of $(\partial E/\partial \log P_0)_j$ obtained by plotting E at 10 mA/cm^2 vs. log P_0 (as shown in Fig. 10) and the value of b in eqn. (3) than to obtain them from the log j_0 vs. log P_0 plots, because of the small variation of Tafel slopes with pressure. The reaction orders thus calculated are about 1 for Pt, Pt + Ni and Pt + Co and about 1.5 for Pt + Cr (Table 4). These values indicate that Pt + Cr may have an electrocatalytic mechanism which is different from that on Pt + Ni and Pt + Co.

PEMFC performance with alloy electrocatalysts

Figure 11 shows the H_2/O_2 PEMFC performances (single cells) with Pt and the three Pt alloy electrocatalysts for the ORR at 95°C and 5 atm. The single cell with the Pt + Cr alloy exhibits the best performance and it is followed by the cell with Pt + Co and then that with Pt + Ni. The cells with the Pt + Co and Pt + Ni alloys exhibit mass transport effects at current densities above 2 A cm^{-2} but such effects are only observed at higher current densities (above 3 A cm^{-2}) in the cells with

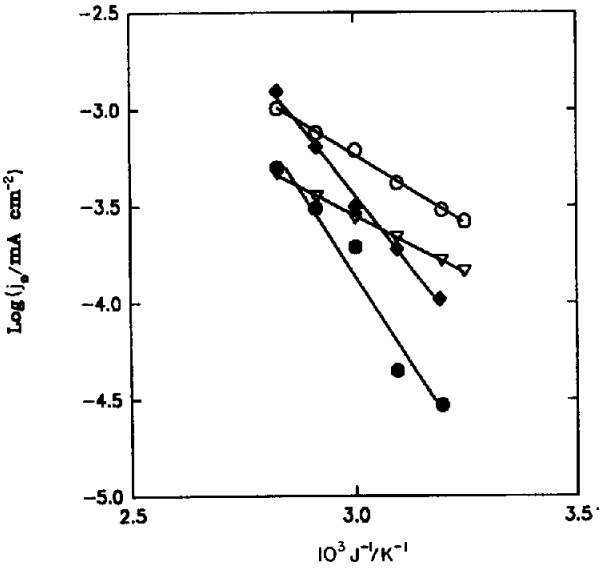

Fig. 6. Arrhenius plots for oxygen reduction on Pt and binary alloys of Pt in proton exchange membrane fuel cells: Pt (●), Pt+Ni (○), Pt+Co (◆) and Pt+Cr (▽).

Pt + Cr and Pt electrocatalysts. This mass transport problem is unrelated to the electrocatalytic behavior of the alloys and is probably due to an artifact during the preparation of the membrane and electrode assemblies, which affects the performance of the cells only at high current densities.

Lifetime and stability of alloy electrocatalysts in PEMFCs

One of the most important facets in using Pt alloys for oxygen reduction is related to its ability to sustain its electrocatalytic enhancement over long periods of

TABLE 4

Structural parameters of carbon-supported Pt alloy electrocatalysts and their electrode kinetic parameters for the ORR in PEMFCs

Electrocatalyst	Lattice parameter/Å	ΔE_a* kJ mol^{-1}	$R(\delta \log j_{900}/\delta T^{-1})$/ kJ mol^{-1}	nO_2 [a]	$(\delta E_{10}$ [b]$/\delta \log P_0)$/ mV	Tafel slope/ mV decade^{-1}	nO_2 [c]
Pt	3.927	75.9	64.64	1.01	62.34	61.5	1.01
Pt+Ni	3.812	27.5	21.46	0.78	60.42	69.5	0.87
Pt+Cr	3.877	23.2	28.19	1.08	86.25	58.0	1.49
Pt+Co	3.854	57.0	24.82	0.77	54.63	63.5	0.86

[a] Reaction order calculated from the slopes of the plot of log j_0 vs. log P_0.
[b] Potential at 10 mA cm^{-2}.
[c] Reaction order calculated using eqn. (3).

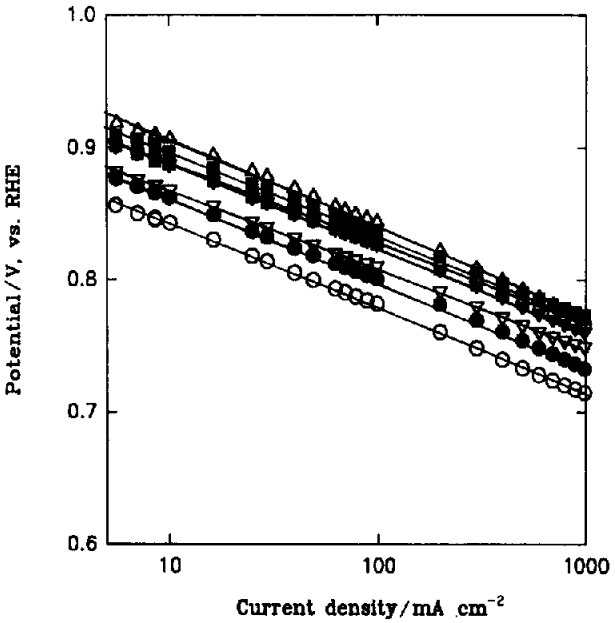

Fig. 7. Dependence of *IR*-corrected Tafel plot on pressure for oxygen reduction at a Pt electrocatalyst in a proton exchange membrane fuel cell: cell temperature, 70°C; pressure, 0.67 (○), 1.37 (●), 2.05 (▽), 2.72 (▼), 3.41 (□), 4.12 (■) and 4.77 (△) atm.

time. For this purpose, the lifetimes were evaluated in single cells at a constant current density of 200 mA/cm^2. The potentials, monitored over a time period range of 400–1200 h, are shown in Fig. 12. There seems to be only a small degradation in the performance of the cells with the Pt + Cr and Pt + C cathodes over an operating time of 1200 h. This result is very similar to an earlier result with a Pt + Ni alloy (same electrocatalyst and Pt loading) [26] up to 1200 h. The Pt + Ni and Pt + Co electrodes, tested over a period of 400 h in this investigation, showed hardly any loss of performance.

SEM / EDXA study (X-ray fluorescence)

To evaluate further the stability of the alloy electrocatalysts, SEM/EDXA examinations were conducted on the anode–membrane–cathode interfaces. The rationale for the EDXA or X-ray fluorescence analysis, rather than the more absolute method of emission spectroscopy, is that the EDXA technique offers a method of determining the concentration of the metal as a function of the distance (on a microscopic scale) in the cross-section of the anode/membrane/cathode assembly. Such an analysis can demonstrate whether or not the more oxidizable alloying component undergoes dissolution at the cathode and migrates to the anode. Secondly, the sensitivity of the emission spectroscopy is not high enough to

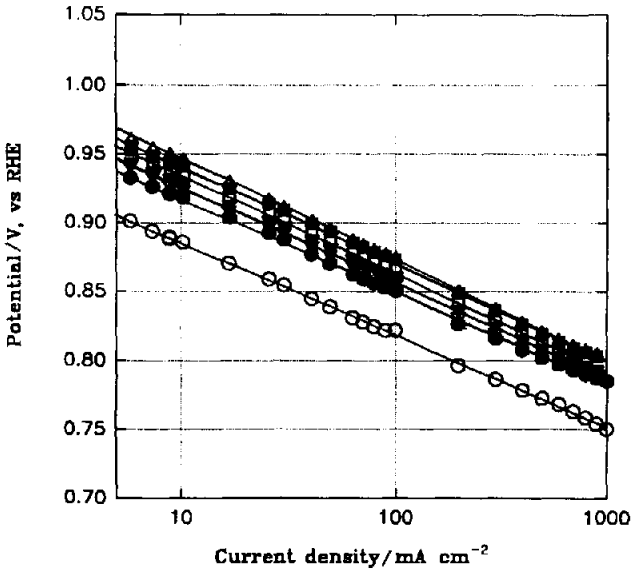

Fig. 8. Dependence of *IR*-corrected Tafel plot on pressure for oxygen reduction at a Pt+Ni alloy electrocatalyst in a proton exchange membrane fuel cell: cell temperature, 70°C; pressure, 0.67 (○), 1.37 (●), 2.05 (▽), 2.72 (▼), 3.41 (□), 4.12 (■) and 4.77 (△) atm.

detect the small amount of loss of the transition metal at the cathode and its migration to the anode.

Figure 13 shows the representative EDXA spectrum of the Pt + Ni alloy electrode at the membrane–cathode electrode interface before and after electrochemical exposure. The samples after electrochemical exposure were those from the cells used for the electrochemical lifetime measurements. The electrochemical exposure times ranged from 400 h in the case of Pt + Ni and Pt + Co to 1200 h for the Pt + Cr alloy electrode. The typical EDXA spectrum shown in Fig. 13 indicates the presence of K shell fluorescence peaks of carbon and fluorine; these peaks correspond to the reaction layer–Teflonized carbon-supported structure at the interface with the Dow membrane. The K shell fluorescence of the sulfur and fluorine peaks indicates the presence of the membrane. There are two peaks for Pt; the large peak overlapping with the Au standard represents the fluorescence from the M shell. The second smaller Pt peak denotes the L shell fluorescence. The peak for Ni corresponds to the K shell fluorescence.

The ratio of the amount of alloying component to the amount of Pt was measured in relation to the carbon (assuming no corrosion of the carbon support, which is a reasonable assumption based on the cell operation at 200 mA/cm^2). The Pt/Ni ratio measured before and after electrochemical exposure was found to be invariant at 3(Pt):1(Ni). The peaks for Ni and Pt, used for this purpose, were for the K and L shell fluorescences. Similar analysis for the Co and Cr indicated no difference between these ratios before and after the electrochemical exposure.

TABLE 5

Effect of pressure on electrode kinetic parameters for oxygen reduction on Pt and Pt alloy electrocatalyst in proton exchange membrane fuel cells

Electrocatalyst	O_2 pressure corrected/atm	E_0/mV	b/mV/decade^{-1}	R/Ω cm^2	E_{10} [a]/mV
Pt	0.67	907	58	0.28	843
	1.37	923	62	0.28	860
	2.05	932	63	0.25	882
	2.72	950	64	0.25	870
	3.41	957	65	0.23	882
	4.09	960	65	0.22	887
	4.77	975	65	0.19	899
Pt+Ni	0.67	951	65	0.15	886
	1.37	981	67	0.13	918
	2.05	992	67	0.12	923
	2.72	999	70	0.12	935
	3.41	1006	72	0.12	938
	4.09	1015	73	0.11	940
	4.77	1019	74	0.11	946
Pt+Cr	0.67	932	54	0.15	869
	1.37	945	56	0.15	886
	2.05	972	57	0.12	907
	2.72	982	57	0.12	916
	3.41	989	59	0.12	929
	4.09	994	59	0.12	933
	4.77	998	62	0.12	939
Pt+Co	0.67	947	59	0.15	888
	1.37	972	62	0.13	908
	2.05	979	64	0.13	920
	2.72	990	65	0.13	925
	3.41	997	66	0.12	929
	4.09	999	68	0.12	932
	4.77	1004	68	0.12	935

[a] Potential at 10 mA cm^{-2}.

Analysis of the EDXA spectrum, in terms of the ratios of the carbon K shell fluorescence to the K shell fluorescence of the alloying element (such as Ni in Fig. 13), indicated negligible dissolution of the alloying component (Table 6). This was also the case for the Pt + Co alloy. The highest dissolution was 5% for the Pt + Cr alloy over a period of 1200 h (Table 6).

XPS analysis

The XPS analysis was conducted to determine the nature of the surface active species, primarily because of the short escape depths of the X-ray photoelectron from the surface (200 Å). This analysis was also used to determine any change in

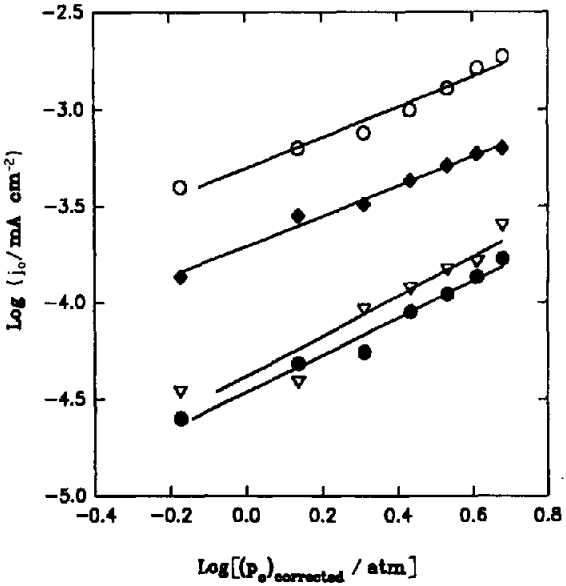

Fig. 9. Plots of exchange current density vs. pressure for oxygen reduction on Pt and Pt alloys in proton exchange membrane fuel cells at 70°C: Pt (●), Pt+Ni (○), Pt+Co (◆) and Pt+Cr (▽).

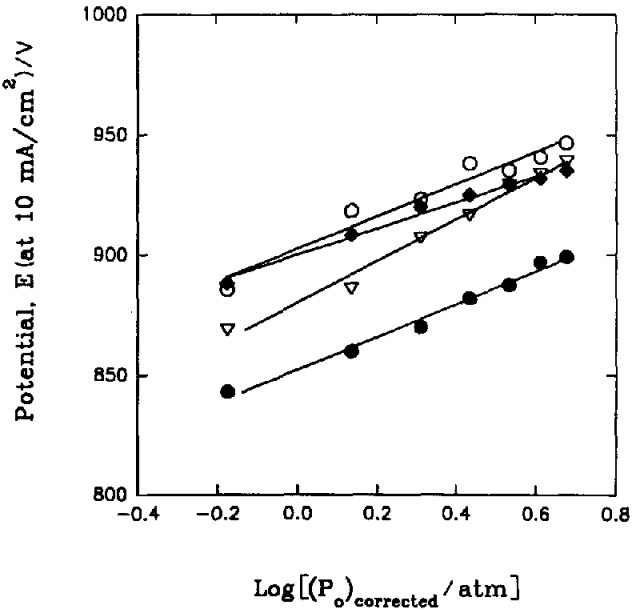

Fig. 10. Plot of E_0 vs. log P_0 for oxygen reduction on Pt and Pt alloys in proton exchange membrane fuel cells at 70°C: Pt (●), Pt+Ni (○), Pt+Co (◆) and Pt+Cr (▽).

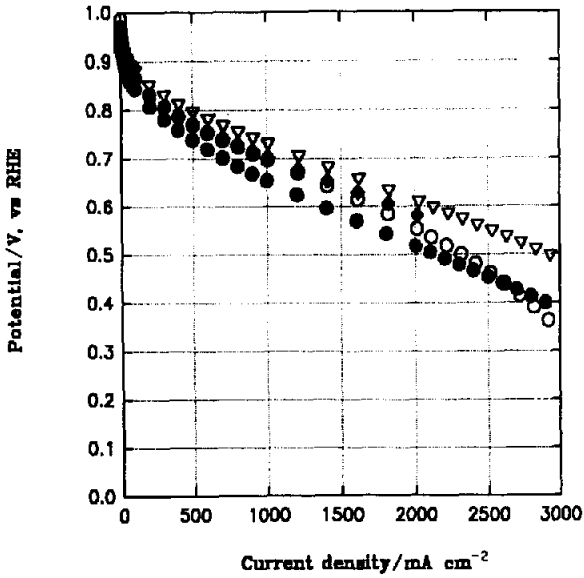

Fig. 11. H_2/O_2 proton exchange membrane fuel cell performances with Pt and Pt alloy electrocatalysts for oxygen reduction: temperature, 95°C; pressure, 5 atm; Pt (●), Pt+Ni (○), Pt+Co (♦) and Pt+Cr (▽).

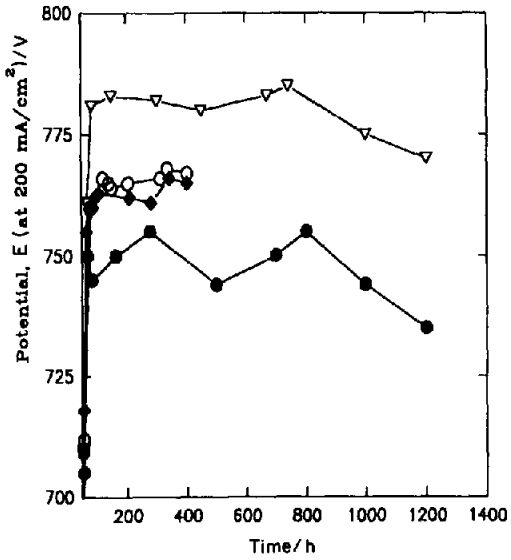

Fig. 12. Lifetime evaluations of Pt and Pt alloy electrocatalysts for oxygen reduction in proton exchange membrane fuel cells: current density, 200 mA cm^{-2}; 50°C; ambient pressure; Pt (●), Pt+Ni (○), Pt+Co (♦) and Pt+Cr (▽).

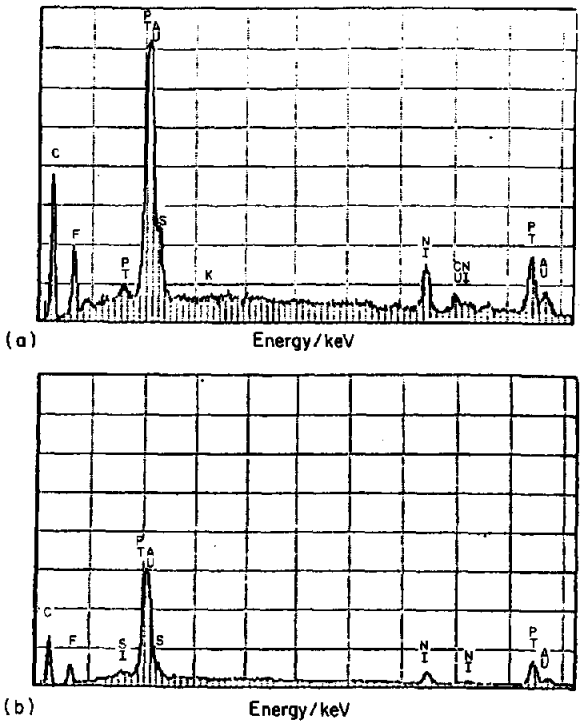

Fig. 13. EDXA spectrum of the cathode electrode–membrane interface with a Pt + Ni alloy electrocatalyst: (a) electrode prior to electrochemical exposure; (b) electrode after 400 h proton exchange membrane in a fuel cell environment. Cell operating conditions: 50°C; 1 atm; current density, 200 mA cm^{-2}.

valence shell electrons due to alloying. The speculation that changes could occur was motivated because alloying of Pt with group V and VI transition metals, as described in the Engel–Brewer bond model [27], can cause a sharing of Pt–d electrons with the unfilled d orbitals of the base metal. Since most of the classical

TABLE 6

X-ray fluorescence analysis of supported Pt and binary Pt alloy electrodes (Pt content in electrode, 0.3 mg cm^{-2}) before and after electrochemical exposure

Electrocatalyst	Electrochemical exposure/h	M [a](Kα)/C(Kα)		Loss of alloying component/%
		Before	After	
Pt + Ni	400	0.029	0.028	3
Pt + Cr	1200	0.033	0.031	5
Pt + Co	400	0.043	0.042	3

[a] Alloying components Ni, Cr and Co.

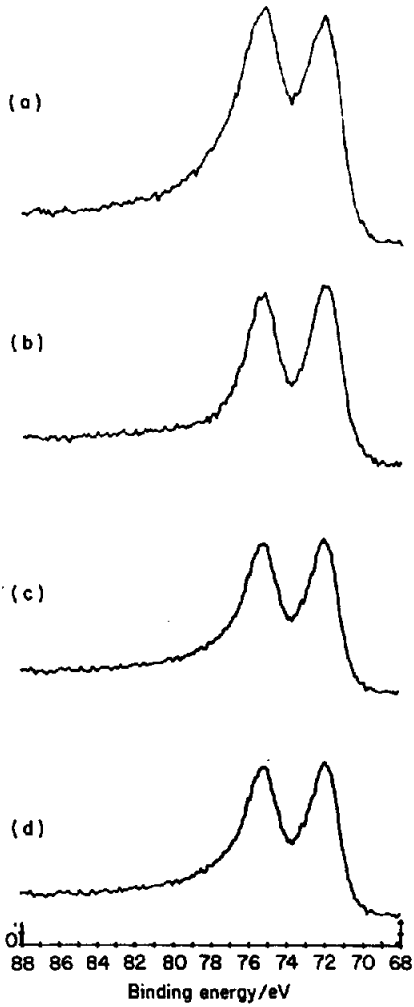

Fig. 14. Pt $4f_{7/2}$ and $4f_{5/2}$ peaks for (a) Pt+C (b) Pt+Cr (c) Pt+Co and (d) Pt+Ni alloy electrocatalysts. All electrocatalysts had 20% metal crystallites on high surface area carbon (Vulcan XC-72).

theories of metal catalysis ascribe the unique catalytic properties of Pt to the d electrons, it would be of great interest to find out if any change in the electronic properties were responsible for the observed oxygen electrocatalysis of these alloys.

Examinations of the XPS spectra indicate that the peak positions for $4f_{5/2}$ and $4f_{7/2}$ are the same in the Pt + C and Pt_3M + C supported electrocatalysts (Fig. 14). This result therefore reveals that there is no change in the Pt valence shell electrons as a result of the alloying process. In other words, Pt retains its electronic

properties in the alloy lattices. The Pt $4f_{7/2}$ and $4f_{5/2}$ peak positions in the supported Pt + C and Pt_3M + C electrocatalysts were at 72.4 and 75.7 eV, indicating the presence of PtO on the surface (a similar analysis of the O 1s XPS line led to the same conclusion). The peak positions of C 1s remained the same (at 284.6 eV) for all the samples and is evidence for the absence of metal–support interactions. The Co $2p_{3/2}$ peak position at 780.6 eV suggests the presence of oxide (CoO) on the surface. The peak position was also the same for a Co electrocatalyst supported on carbon (20% Co on carbon, ETEK, Framingham, MA). The Co $2p_{3/2}$ peak positions for the Pt + Co alloy electrocatalyst and the Co + C supported catalyst were identical.

These studies show that Co mainly exists on the surface as an oxide. The Cr $2p_{1/2}$ and $2p_{3/2}$ peaks for the Pt + Cr alloy samples were at 586 and 576 eV, indicating the presence of Cr_2O_3. This result is also supported by previous results of Daube et al. [28]. Furthermore, an electrocatalyst with 20% Cr on carbon also exhibited the same peak position as that in the Pt + Cr alloy. This again indicates that Cr is predominantly present as Cr_2O_3 on the surface. The Pt + Ni alloy also did not reveal any peak position shifts with respect to Pt $4f_{7/2}$ and $4f_{5/2}$ (see Fig. 14). A comparison of the peak positions of Ni $2p_{1/2}$ and $2p_{3/2}$ in the Pt + Ni alloy and in the 20%Ni + C reference sample (ETEK) showed peaks at 853.3 eV ($2p_{3/2}$) and 871.7 eV ($2p_{1/2}$), indicating the presence of NiO on the surface.

CONCLUSIONS

The present investigation demonstrates clearly a two- to threefold enhancement of the electrocatalytic activity of the ORR at the interfaces of the Pt + Ni, Pt + Cr and Pt + Co alloys with proton exchange membranes under the PEMFC operating conditions. The enhancements were much greater on the basis of the electrochemically active surface area of Pt (Table 2). These results can be rationalized on the basis of the existence of the superlattices of Pt_3Cr, Pt_3Co and Pt_3Ni, all having the same cubic f.c.c. structure as Pt + C but with lattice contractions (Tables 1 and 4).

The particle size analysis revealed that, despite an increase in the particle size (and hence a decrease in surface area), the specific activities for the ORR were higher on the alloys than that on Pt. The activation energies, determined by measuring the exchange current densities over the temperature range 35–80°C, indicate significantly lower values for the alloys than that on Pt/C (Table 4). By an analysis of the dependence of the exchange current densities for the ORR on the pressure of oxygen, the values of the reaction orders were found to be unity for Pt and Pt + Cr but were about 0.8 for Pt + Ni and Pt + Co. An alternative analysis from the variation of the potential at 10 mA/cm^2 with oxygen pressure, indicated a reaction order of 1.5 on Pt + Cr, and of unity on Pt + Co, Pt + Ni and Pt, (Table 4).

The discrepancies in the results obtained by these two approaches (exchange current density vs. E_{10} mA/cm^2) arises because the evaluation of the exchange current density involves extrapolation over several decades of current density and

is exponential in nature. Therefore, it would be more realistic to consider the values at 900 mV vs. RHE (for activation energy evaluation) and potential at 10 mA/cm^2 (for the evaluation of reaction order), both of which lie well within the activation-controlled region. However, the evaluation of the reaction order and the activation energy using exchange current density as well as current density at 900 mV vs. RHE and potential at 10 mA cm^{-2} for the carbon-supported Pt electrocatalyst showed good agreement with previously reported values [18].

The lifetime studies on these electrocatalysts in PEMFCs showed only negligible losses in performance, as confirmed by the SEM/EDXA examinations of the cathode electrode/Dow membrane interface. The XPS investigation revealed the presence of oxide layers on the surface of the as-received electrocatalysts. Furthermore, the absence of any chemical energy shifts in the XPS of the alloy electrocatalyst powders negates any significant electronic transitions owing to alloying, in contrast to that predicted by the Engel–Brewer-type bond model. However, it is too early to make any final conclusions in this regard. Studies using in situ X-ray analysis of near-edge structure and extended X-ray analysis fine structure are in progress to shed further light on the explanations for the enhanced activities on the Pt alloy electrocatalysts.

ACKNOWLEDGEMENTS

This work was carried out under the auspices of the National Aeronautical and Space Administration-Johnson Space Center (Regional University Grant NAG 9-533) and is in the partial fulfillment of the requirements for the PhD degree in Chemistry by one of us (SM). The authors wish to thank Prof. Manuel P. Soriaga, Dr. A. Cesar Ferriera and Mr. Omourtag A. Velev for valuable discussions and suggestions and/or initial assistance in the experimental work. One of us (SM) is on leave of absence from the Tata Energy Research Institute, New Delhi, India.

REFERENCES

1 J.O'M. Bockris and S. Srinivasan, Fuel Cells: Their Electrochemistry, McGraw-Hill, New York, 1969.
2 D.A. Landsman and F.J. Luczak, US Patent 4,316,944 (1982).
3 V.M. Jalan and E.J. Taylor, in J.D.E. McIntyre, M.J. Weaver, and E.B. Yeager (Eds.), The Chemistry and Physics of Electrocatalysis, The Electrochemical Society, Pennington, NJ, 1984, p. 546.
4 L. Christener and M. Farooque, Contract DEN 3-205, NASA CR-174660 (March 1994).
5 V.M. Jalan and E.J. Taylor, J. Electrochem. Soc., 130 (1983) 2299.
6 A.J. Appleby, Catal. Rev., 4 (1970) 221.
7 J.T. Glass, G.L. Cahen and G.E. Stoner, J. Electrochem. Soc., 134 (1987) 58.
8 M.T. Paffett, J.G. Beery and S. Gottesfeld, J. Electrochem. Soc., 135 (1988) 1431.
9 J.A.S. Bett, in D. Scherson, D. Tryck, M. Deroux and X. Xing (Eds.), Proc. Symp. on Structural Effects in Electrocatalysis and Oxygen Electrochemistry, PV 92-11, The Electrochemical Society, Pennington, NJ, 1992, p. 573.
10 A.J. Appleby, Energy, 11 (1986) 13.

11 E.A. Ticianelli, C.R. Derouin and S. Srinivasan, J. Electrochem. Soc., 251 (1988) 275.
12 J.G. Beery, E.A. Ticianelli and S. Srinivasan, J. Appl. Electrochem., 21 (1991) 597.
13 W. Pearson, A Handbook of Lattice Spacings and Structure of Metals and Alloys, Vol. 4, Pergamon, Oxford, 1986.
14 U. Bardi, D. Dahlgren and P.N. Ross, J. Catal., 100 (1986) 196.
15 U. Bardi, B. Beard and P.N. Ross, J. Catal, 124 (1990) 22.
16 A. Haner and P.N. Ross, J. Phys. Chem., 95 (1991) 3740.
17 S. Srinivasan, E.A. Ticianelli, C.R. Derouin and A. Redondo, J. Power Sources, 22 (1988) 359.
18 A. Parthasarthy, S. Srinivasan, A.J. Appleby and C.R. Martin, J. Electroanal. Chem., 339 (1992) 101.
19 T. Swanson, Natl. Bur. Stand., (US), Circ., 539 (1953) 131.
20 A. Kuzzman and H.E.V. Steinwehr, Z. Metallkd., 40 (1949) 263.
21 J. Baglin, J. Electrochem. Soc., 125 (1978) 1854.
22 A.H. Geisler and D.L. Martin, J. Appl. Phys. 23 (1952) 37.
23 H. Klug and L. Alexander, X-ray Diffraction Procedures, Wiley, New York, 1962, p. 491.
24 L.V. Azaroff, Elements of X-ray Crystallography, McGraw-Hill, New York, 1968, p. 556.
25 B. Culity, Elements of X-ray Diffraction, Addison Wesley, Reading, MA, 1956, p. 366.
26 S. Srinivasan, O.A. Velev, A. Parthasarthy, D.J. Manko and A.J. Appleby, Final Rep., NASA-JSC (Grant NAG 9-533) (1991).
27 L. Brewer, in P. Rudman, J. Stringer, and R. Jaffer (Eds), Phases Stability in Metals and Alloys, McGraw-Hill, New York, 1967, p. 39.
28 K.A. Daube, M.T. Paffett, S. Gottesfeld and C.T. Campbell, J. Vac. Sci. Technol. A, 4(3) (1986) 1617.